



Acoustic emission characteristics of a fine-grained marble with different thermal damages and specimen sizes

Jun Peng^{1,2} · Guan Rong¹ · Mengdi Yao¹ · Louis Ngai Yuen Wong^{3,4} · Zhicheng Tang⁴

Received: 30 April 2018 / Accepted: 18 August 2018 / Published online: 3 September 2018
© Springer-Verlag GmbH Germany, part of Springer Nature 2018

Abstract

Acoustic emission (AE) is a technique which has been widely used in geomechanics to study the progressive micro-cracking behavior of rocks in response to different loadings. However, the study of the combined effects of thermal damage and specimen size on the performance of rocks using the AE technique is still limited, which needs further investigation. This study experimentally investigated the AE characteristics of a fine-grained marble with different thermal damages and specimen sizes. The variation of AE counts in response to the rock deformation can divide the stress–strain relation into several stages. The AE activity is limited in the initial deformation stage and multiplies at a stress level about 0.7 to 0.8 times the peak stress. However, the AE signals in the initial stage become more prominent as the treatment temperature increases. The accumulated AE parameters (i.e., AE counts, AE hits, and AE energy) are found to decrease with the increase in the treatment temperature. The *b*-value, which generally decreases as the stress approaches the peak strength, correlates well with the stress–strain relation. It is also found that the *b*-value generally increases as the treatment temperature gradually increases, which is mainly attributed to the initially generated thermal micro-cracks in the rock specimen. The real-time spatial distribution of AE events is in considerable agreement with the failure mode observed in laboratory tests. Overall, the results in this study reveal that the AE technique is capable of studying the micro-cracking behavior involved in the deformation process of rocks possessing different degrees of thermal damage and with different specimen sizes.

Keywords Acoustic emission (AE) · Thermal damage · Specimen size · *b*-Value · Source location · Micro-cracking evolution

Introduction

Understanding and predicting the strength and deformation behavior of rocks is an important topic in geomechanics, which can facilitate cost-effective design and long-term stability of engineering structures, such as deep tunnels for mining, boreholes for oil or gas production, tunnels for the storage of

radioactive waste, and wells for the injection of carbon dioxides. Numerous laboratory test results have revealed that the deformation (failure) of rocks is, to a large extent, attributed to the closure, initiation, propagation, and coalescence of micro-cracks inside the rock specimens (Bieniawski 1967; Brace et al. 1966; Cai et al. 2004; Diederichs and Martin 2010; Diederichs et al. 2004; Eberhardt et al. 1998; Lajtai and Lajtai 1974; Martin and Chandler 1994; Wong and Einstein 2009a, b; Zhao et al. 2015). The associated micro-cracking processes can divide the rock deformation into several distinct stages from crack closure to crack coalescence (Brace et al. 1966; Martin and Chandler 1994). It is, therefore, of vital importance to study the strength and deformation behavior of rocks from a microscopic view.

In the last several decades, many researchers have studied rock strength and the associated micro-cracking behavior using various microscopic observation techniques. These techniques include scanning electron microscope (SEM) (Tapponnier and Brace 1976), X-ray computed tomography (CT) (Vinegar et al. 1991), acoustic emission (AE) (Lockner

✉ Guan Rong
rg_mail@163.com

¹ State Key Laboratory of Water Resources and Hydropower Engineering Science, Wuhan University, Wuhan 430072, China

² State Key Laboratory for Geomechanics and Deep Underground Engineering, China University of Mining and Technology, Xuzhou 221008, China

³ Department of Earth Sciences, The University of Hong Kong, Hong Kong, China

⁴ Faculty of Engineering, China University of Geosciences, Wuhan 430074, Hubei, China

et al. 1991), and high-speed camera (Wong and Einstein 2009a, b). Among these techniques, AE is a method which has been proven to be useful particularly for studying the progressive micro-cracking behavior of rock specimens during loading (Chen et al. 2017; Fu et al. 2015; He et al. 2010; Jansen et al. 1993; Lei et al. 2000; Liu et al. 2017; Meng et al. 2017; Slatalla et al. 2010; Yan et al. 2016; Zhao and He 2017; Zhao et al. 2013). Due to its high sensitivity to micro-cracking, AE monitoring has also been used to provide early warning signals with great success in the construction of large-scale engineering structures, such as deep tunnels for hydropower stations or mining (Alcott et al. 1998; Butt et al. 2000; Dai et al. 2016; Goodfellow and Young 2014; Xu et al. 2016, 2017).

AE can be defined as the transient elastic wave generated by the rapid release of energy from a source within a material (Koerner et al. 1981; Mansurov 1994). The AE activity in a rock generally initiates from micro-cracking which is associated with dislocations, grain boundary movement, or the initiation, propagation, and coalescence of micro-cracks through and between mineral grains (Eberhardt et al. 1998). It correlates well with the micro-cracking behavior involved in different stages of the stress–strain relation. A schematic illustration of the AE method used for the examination of micro-crack development in a rock specimen under loading is shown in Fig. 1.

The AE signal recorded by the AE transducer is first amplified in a pre-amplifier and then transferred to a data logger and subsequently compute for analysis. A threshold value is usually applied to the recorded AE data to filter out the background noises. AE parameters, such as (transient or accumulated) AE count and AE hit, have been widely used to correlate the stress–strain relation with the micro-cracking process in the rock specimen (Eberhardt et al. 1999; Lockner 1993; Scholz 1968a). In addition, some waveform parameters involved in the generation of an AE event, such as ring-down count, energy, peak amplitude, rise-time, and event duration,

also provide useful information to further elucidate the micro-cracking mechanisms associated with the macroscopic deformation and failure of rocks (He et al. 2010; Zhao et al. 2014). In general, one signal received by a transducer that exceeds the threshold is termed as one hit. One signal received by at least four transducers is termed as one event. The oscillation number of a pulse signal crossing the threshold is the AE count (short for AE ring-down count). The definitions of these AE parameters illustrated in Fig. 1 can also be referred to in Eberhardt et al. (1998).

The AE monitoring technique has been widely and successfully used in recent years to investigate the brittle failure and the associated micro-cracking behavior of various rock types (see Table 1). For a meaningful comparison of previous studies, the collected test data in Table 1 are exclusively based on compressive loading tests on cylindrical specimens, while test data of other specimen shapes are not included. The reviewed rock specimens generally have a height-to-diameter ratio of 2 to 2.5, with the diameter ranging from 20 to 75 mm. The number of sensors used in these studies ranges from one to 32, while four and eight are the most common. Some advanced analysis methods involving AE monitoring have also been used in rock mechanics, including moment tensor inversion, source location, *b*-value analysis, and fractal characteristics.

Thermal damage is a factor which significantly affects the rock strength and deformation behavior (Liu et al. 2017; Peng et al. 2016a, b; Rong et al. 2018a, b; Sirdesai et al. 2017a, b, c, 2018a, b). The mechanical behavior and AE characteristic of rocks are also greatly influenced by the specimen size (Hawkins 1998). The combined influences of thermal damage and specimen size on the physical and macroscopic mechanical behavior of a fine-grained marble have recently been experimentally investigated by Rong et al. (2018c). Their results show that the thermal damage and specimen size greatly

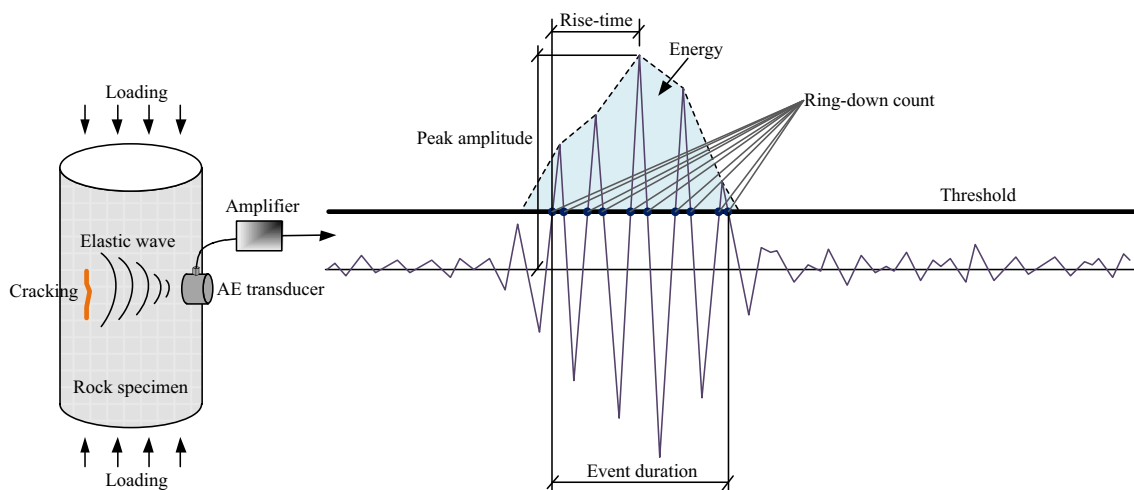


Fig. 1 Illustration of transient elastic wave generation and acoustic emission (AE) characteristics during compressive loading of a rock specimen (reproduced from Zhao et al. 2013)

Table 1 Summary of recent acoustic emission (AE) studies on cylindrical rock specimens under compressive loading in laboratory tests

No.	Rock type	Specimen size, $D * H$ (mm)	No. of sensors	Gain (dB)	Threshold (dB or V)	Methods	References
1	KURT granite	52 * 124.1	8	60	65 ^a	Moment tensor, <i>b</i> -value	Kim et al. (2015)
2	North Africa gabbro	40 * 90	4	40	45 ^a	AE parameter	Keshavarz et al. (2010)
3	Beishan granite	50 * 100	6	40	40 ^a	Source location, AE parameter	Zhao et al. (2013)
4	Hwangdeung granite, Yeosan marble	50 * 100	6	40	45 ^a	Moment tensor, source location	Chang and Lee (2004)
5	Vosges sandstone	50.8 * 127	12	/	/	Moment tensor, source location	Aker et al. (2014)
6	Biotite monzogranite	50 * 100	8	/	40 ^a	Source location, fractal analysis	Zhang et al. (2015a)
7	Xinzhi sandstone	50 * 100	/	/	/	Source location, AE energy	Kong et al. (2016)
8	Strathbogie granite	22.5 * 45	/	/	/	Cumulative AE counts	Shao et al. (2015)
9	Halite, glauberite, and gypsum	50 * 100	4	30	60 or 40 ^a	AE parameter	Zhang et al. (2015b)
10	Linyi granite	20 * 45	1	35	35 ^a	AE parameter	Zhai et al. (2013)
11	Jinping marble	50 * 100	8	40	45 ^a	Source location	Pei et al. (2013)
12	Lac du Bonnet granite	61 * 137.3	4	40	0.1 ^b	AE parameter	Eberhardt et al. (1997)
13	Porphyry, granite, and concrete	50 * 100	32	20	45 ^a	Source location, <i>b</i> -value, fractal analysis	Lei et al. (2004)
14	Granite, granodiorite, and pegmatite	61 * 137.3	4	40	0.1 ^b	AE parameter	Eberhardt et al. (1999)
15	Red sandstone	50 * 100	8	/	33 ^a	Source location	Yang et al. (2012)
16	Rock salt	75 * 150	8	40	35 ^a	Source location, fractal analysis	Xie et al. (2011)
17	Beishan granite	50 * 100	8	40	30 ^a	Source location, cumulative AE counts	Chen et al. (2015)
18	Kaliningrad and Tula rock salt	40 * 80 to 90	1	40	0.1 ^b	AE count rate	Filimonov et al. (2001)
19	Zhenping marble	50 * 100	4	40	50 ^a	Source location, AE parameter	Guo et al. (2015)
20	Dholpur sandstone	40 * 80	2	/	60 ^a	AE parameter	Sirdesai et al. (2018a)

“/” denotes that the data are not provided in the publication. Under “Threshold”, superscript ^a represents the data in the unit of dB and superscript ^b denotes the data in the unit of V

influence the physical and mechanical properties, such as P-wave velocity, micro-crack density, stress–strain curves, rock strength, Young’s modulus, and failure mode. The previous experimental studies on the effects of thermal damage and specimen size on the performance of rocks are comprehensively reviewed in their study, which will not be presented here. Interested readers can refer to the paper for more details. In the present study, the AE characteristics of a fine-grained marble with different thermal damages and specimen sizes are investigated. The results of AE parameter, *b*-value evolution, and source location are examined and analyzed.

Experimental design

Experimental setup

The marble studied in this study is a fine-grained metamorphic rock. It was collected from a mine located in Pingnan City of Fujian Province, China, which is the same as that investigated by Rong et al. (2018c). It is mainly composed of dolomite, accounting for 96.0% of its total volume, with small amounts of calcite and albite. It has a crystalloblastic texture and massive structure. The texture is relatively isotropic. No visible fractures can be found in the rock sample; however, some dark dykes are developed inside the sample. The grain size of the fine-grained dolomitic marble ranges from 0.5 to 1.0 mm and the porosity is about 1.8%.

Cylindrical specimens with a length-to-diameter ratio of 2 were prepared. Four diameters are associated with these prepared specimens, including 25, 50, 75, and 100 mm. The procedure for thermal treatment is the same as that used by Rong et al. (2018c). A furnace was used to heat the specimens to different temperatures (i.e., 25, 200, 400, and 600 °C), with a heating rate of 10 °C/min. After reaching the predetermined temperature, the specimens were kept in the furnace for 4 h and then taken out to cool down to room temperature naturally. When the specimen was heated to a higher temperature, such as 800 °C, the integrity of the specimen was completely destroyed and it could be broken by hand. Hence, the predetermined temperatures in this study have been limited to a maximum value of 600 °C.

In all uniaxial compression tests, the AE information was recorded using AE detection model PCI-2 of the DISP series manufactured by the American Physical Acoustics Corporation. All uniaxial compression tests were loaded using axial displacement-controlled loading at a rate of 0.075 mm/min. Four AE piezoceramic transducers with a resonance frequency range of 100 to 400 kHz were directly mounted onto the circumferential surface of the specimen. As shown in Fig. 2, two AE transducers (1# and 2#, 3# and 4#) were treated as a group and installed symmetrically in a plane at about a quarter of the height of the specimen. An orthogonal layout of the two groups of transducers provided good coverage of the specimen volume. To achieve a satisfactory acoustic coupling, a thin layer of Vaseline was applied at the interface between

the specimen surface and the AE transducers (Pei et al. 2013; Guo et al. 2015; Zhang et al. 2015b; Zhao et al. 2013). Two loops of rubber band with width comparable to the AE transducer diameter was used to fix the transducers. To check the coupling between AE transducers and the specimen surface, pencil lead fracture tests were conducted before AE monitoring (Guo et al. 2015; Xiong and Wong 2017). Each AE transducer was calibrated to have a minimum amplitude of 95 dB.

The sensitivity of the AE test is, to a large extent, controlled by the gain and threshold of the system (Eberhardt et al. 1998). The signals are pre-amplified for an effective detection of small AE signals induced from micro-cracking in the rock specimen during loading, and the gain is a measure of the amplification provided by the system. On the other hand, the threshold is used to filter out small signals associated with background noise. Therefore, proper choice of these two parameters is important for analyzing AE characteristics. Based on the literature review shown in Table 1, a gain within the range of 20 to 60 dB is normally used in rock tests. In our study, the gain value is set to 40 dB in the pre-amplifier. Two types of thresholds in the units of dB or V are usually used, as shown in Table 1. The threshold in the unit of V can be converted to that in the unit of dB by using the following equation

$$tre(dB) = 20 \log \left(\frac{tre(V)}{10^{-7}} \right) - pre, \quad (1)$$

where $tre(dB)$ and $tre(V)$ are the thresholds in the units of dB and V, respectively, and pre is the gain value of the pre-amplifier in the unit of dB.

Based on the above, the threshold of 0.1 V in Table 1 corresponds to a threshold value of 60 dB. Therefore, the threshold used in previous AE studies ranges from 30 to 65 dB. In this study, the threshold was set to be 45 dB. As shown in later

sections, the assigned gain and threshold values are capable of capturing the AE characteristics of rock specimens of different diameters and treatment temperatures. Full waveform data were sampled at a rate of 2 MHz.

AE data analysis

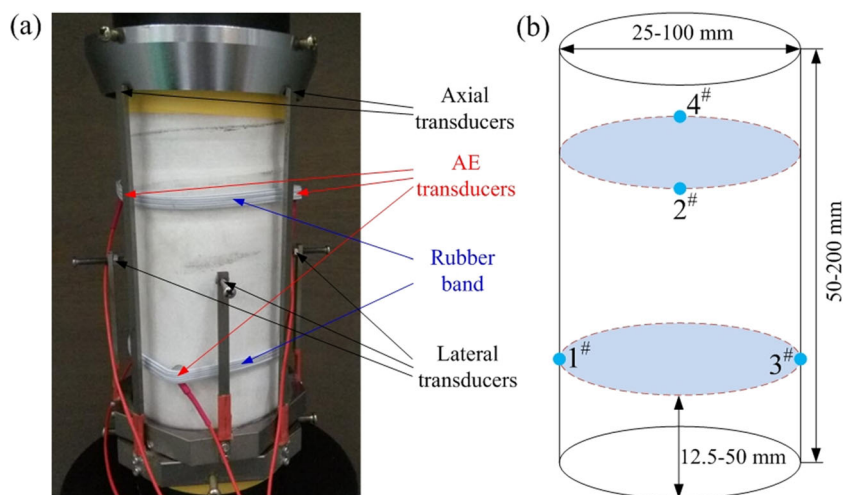
In this study, the AE parameters, including AE counts, AE hits, AE hit rate, AE energy, and waveform data were recorded during the uniaxial compression tests. To have a better understanding of the combined influences of thermal damage and specimen diameter on the AE characteristics, two analyses based on b -value and source location of AE activities were conducted. In the following subsections, the principles of b -value analysis and source location will be introduced.

b -Value

In the field of earthquake seismology, it is generally acknowledged that events of large magnitude occur less frequently as compared with those of small magnitude. Based on the Gutenberg and Richter relationship (Gutenberg and Richter 1942), the b -value can be defined as the log-linear slope of the frequency–magnitude distribution. Because the peak amplitude of AE signals is closely related to the magnitude of the fracture, the b -value is considered as an effective index for evaluation of the fracture process (Mogi 1962; Scholz 1968b). The b -value changes accordingly with the different stages of fracture growth and it has been widely used in recent years to estimate the development of the micro-cracking process in rock mechanics (Kim et al. 2015; Lei et al. 2004). The following equation is generally used to determine the b -value as

$$\log N = a - bM, \quad (2)$$

Fig. 2 Arrangement of AE transducers (1#, 2#, 3#, and 4#) attached to the cylindrical surface of specimens of various dimensions



where M is the Richter magnitude of events, which is basically proportional to the logarithm of the maximum amplitude A_{\max} recorded in a seismic trace, N is the incremental frequency (i.e., the number of events with magnitudes in the range of $M \pm \Delta M/2$), and a and b are empirical constants. The parameter b denotes the widely used b -value.

The b -value can be used, to some extent, to reflect the micro-cracking intensity in the material. In general, a high b -value corresponds to a low micro-cracking rate. On the contrary, a low b -value means that a large amount of micro-cracks is developed at this stage. In this study, the variation of b -value with the normalized axial stress is examined to interpret the micro-cracking process in the rock specimen. An average b -value is calculated using the dataset recorded in the four AE transducers to minimize the error.

Source location

The AE source location is used to retrieve the location of a fracture source through comparing the arrival time of the same P-wave received by different transducers. The evolution of micro-cracks inside a rock specimen can be reflected using the method of source location. The basic principle of the non-linear iterative algorithm in this study is that the location of the fracture source is determined through regressive computation for the time difference of the AE signal arriving at different transducers. The arrival time of each AE event is automatically obtained by the software (AEWIN for PCI-2 software version 1.30). According to the user's manual, the arrival time is defined as the time when the input signal first exceeds a pre-set threshold and is recorded to have an accuracy of $\pm 0.05 \mu\text{s}$. It is generally assumed that the velocity in the material is uniform. Hence, the P-wave velocity is set to be a constant throughout the entire course of a compression test. In this study, the P-wave velocity was set to be 4.8 km/s (Rong et al. 2018c). However, it should be noted that the velocity field is generally anisotropic, induced from the progressive deformation process. Thus, the constant velocity assumption inevitably produced errors. Based on the least squares method, the AE source residual is minimized by continuously improving the AE source to estimate the AE source position. The iterative process of the AE source location is automatically conducted in the AEWIN software.

The distance between the i th transducer and AE source is estimated as

$$\sqrt{(x-x_i)^2 + (y-y_i)^2 + (z-z_i)^2} = v_p(t_i-t), \quad (3)$$

where (x, y, z) are the estimated coordinates of the AE source, (x_i, y_i, z_i) are coordinates of the i th transducer, t is the estimated initiation time of the AE source, t_i is the observed arrival time

at the i th transducer, and v_p is the P-wave velocity in the rock specimen.

The square of the deviation, Q , is expressed as

$$Q = \sum_{i=1}^N \left[\sqrt{(x-x_i)^2 + (y-y_i)^2 + (z-z_i)^2} - v_p(t_i-t) \right]^2, \quad (4)$$

where N is the number of transducers.

The minimum value of the square of the deviation (Q) can be obtained by iterative computations using the least squares method. Three different iteration algorithms, namely the Gaussian method, the modified Gaussian method, and the downhill simplex method, are available for the computation. In general, the minimum number of transducers forming an array is determined by the spatial dimension to be measured. For a cylindrical rock specimen, at least four transducers are required to locate an AE source. As studied by Labuz et al. (1988), four transducers can determine the locations of AE sources with an estimated error of less than 5 mm.

Experimental results

The AE characteristics of rock specimens with different diameters (25, 50, 75, and 100 mm) and different degrees of thermal damage (25, 200, 400, and 600 °C) are compiled and discussed in this section. The obtained AE parameters are first examined, followed by an interpretation of the accumulated AE parameters with temperature. The variation of b -value with the normalized axial stress is then analyzed and discussed. Finally, the micro-cracking evolution using the source location method is examined.

AE characteristics of rock specimens

Specimens with a diameter of 25 mm

The stress–strain relations and the corresponding variations of accumulated AE counts and AE hits with the axial strain for specimens with a diameter of 25 mm are presented in Fig. 3. The results reveal that the evolutions of accumulated AE counts and AE hits can correlate well with the stress–strain relations. For the specimen without thermal damage (25 °C) (see Fig. 3a), almost no AE signals can be recorded in the initial deformation stage. The AE signals initiate at a stress level about 0.4 times the peak strength and multiply at about 0.8 times the peak stress. The accumulated AE counts show a similar trend for specimens with thermal damage (see Fig. 3b–d). However, with the increase in the treatment temperature, the AE signals in the initial stage become more prominent, especially for the specimen thermally treated at 600 °C. This is mainly attributed to more micro-cracks being created at the higher treatment temperature. These initially developed

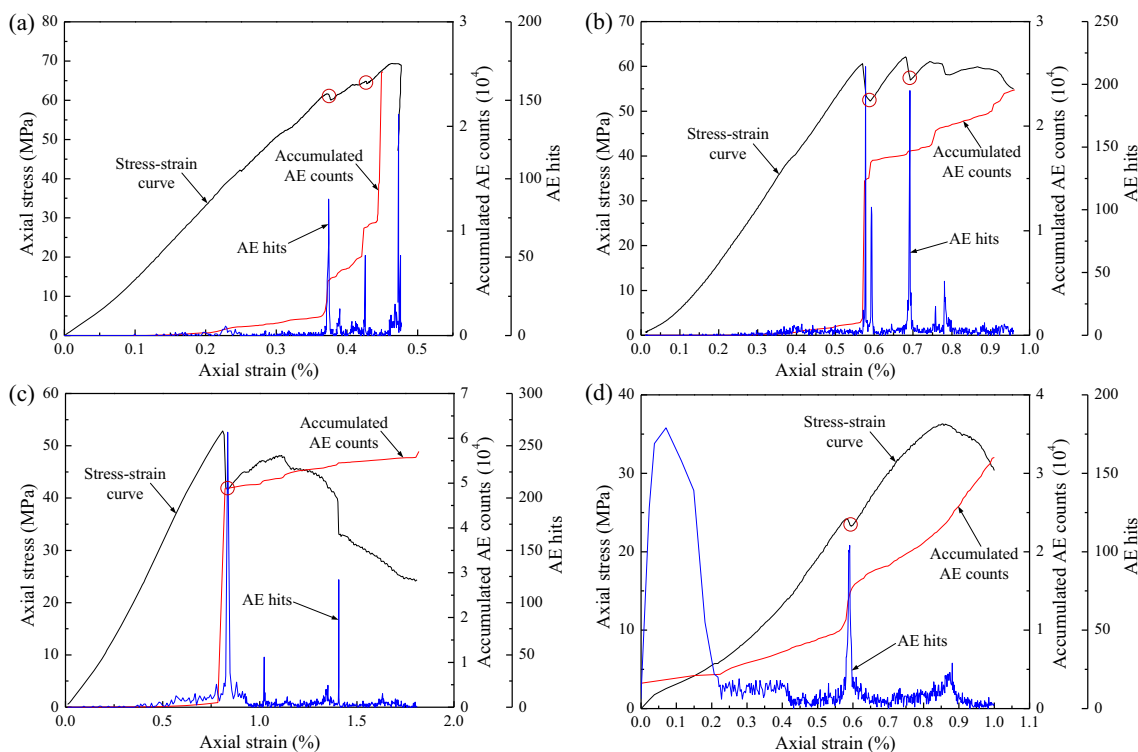


Fig. 3 Evolutions of accumulated AE counts and AE hits with axial strain for rock specimens with 25 mm diameter after thermal treatment with different temperatures. **a** Room temperature (25 °C), **b** 200 °C, **c** 400 °C, and **d** 600 °C

micro-cracks will, hence, become the preferential cracking sites, leading to more dramatic AE activities in the initial deformation stage.

Occasional stress drops are observed on the stress–strain curves in Fig. 3 (see the red circles). The corresponding AE signals recorded at this stage also show a drastic increase. This phenomenon is generally attributed to the dislocation or breakage of minerals or grain boundary movement in the rock specimen during loading. The sudden slip or breakage of minerals along the grain boundaries will induce a transient stress relaxation, which will result in a sudden stress drop in the stress–strain curve and lead to a large amount of AE activities.

Specimens with a diameter of 50 mm

Figure 4 shows the stress–strain relations and the corresponding variations of accumulated AE counts and AE hits with the axial strain for specimens with a diameter of 50 mm. The results are considerably comparable with those of specimens with a diameter of 25 mm. The evolutions of accumulated AE counts and AE hits show good correlation with the stress–strain behavior. Few AE signals are detected in the initial deformation stage and the accumulated AE counts start to multiply at a stress level about 0.8 times the peak strength. Similarly, the AE signals in the initial stage will become more prominent with the increase in the treatment temperature. In addition, the phenomenon of “sudden stress drop” can also be

observed in the pre-peak or post-peak deformation of the specimen, which corresponds to a quick AE signal increase. These points denote the dislocation or breakage of minerals or grain boundary movement in the rock specimen during loading.

On the other hand, more accumulated AE counts and AE hits of specimens with a diameter of 50 mm can be observed when compared with those of specimens with a diameter of 25 mm. The numbers of these two parameters for specimens with a diameter of 50 mm are about 2 to 3 times greater than those for specimens with a diameter of 25 mm.

Specimens with a diameter of 75 mm

The stress–strain relations and the corresponding variations of accumulated AE counts and AE hits with the axial strain for specimens with a diameter of 75 mm are shown in Fig. 5. The results reveal that, similar to the results of specimens with diameters of 25 and 50 mm, the evolutions of accumulated AE counts and AE hits show good correlation with the micro-cracking process in the rock specimens (i.e., stress–strain behavior). The AE signals initiate at a stress level about 0.3 to 0.4 times the peak stress and multiply at a stress level about 0.7 to 0.8 times the peak stress. A great increase of AE signals in the initial deformation stage is also observed for the rock specimen thermally treated under the temperature of 600 °C. Meanwhile, the “sudden stress drop” phenomenon can also be observed for specimens under the temperatures of 25, 200,

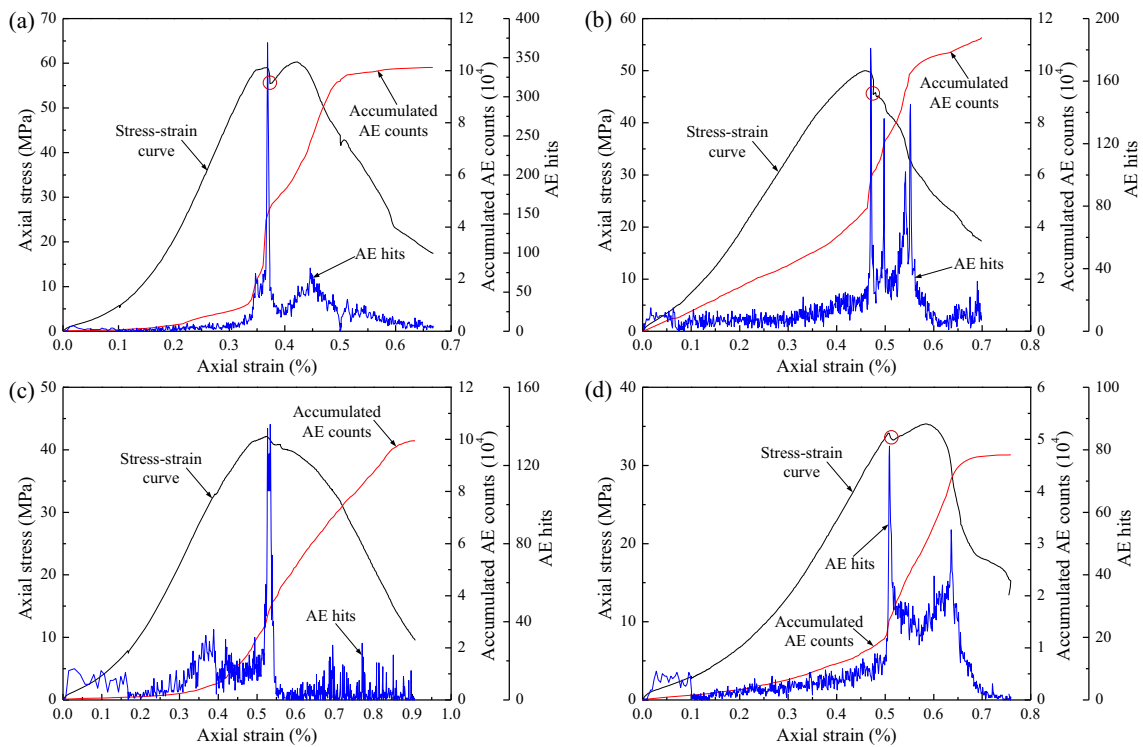


Fig. 4 Evolutions of accumulated AE counts and AE hits with axial strain for rock specimens with 50 mm diameter after thermal treatment with different temperatures. **a** Room temperature (25 °C), **b** 200 °C, **c** 400 °C, and **d** 600 °C

and 400 °C, which denotes the dislocation or breakage of minerals or grain boundary movement in the rock specimen.

When compared with the results of specimens with a diameter of 50 mm, though the number of accumulated AE

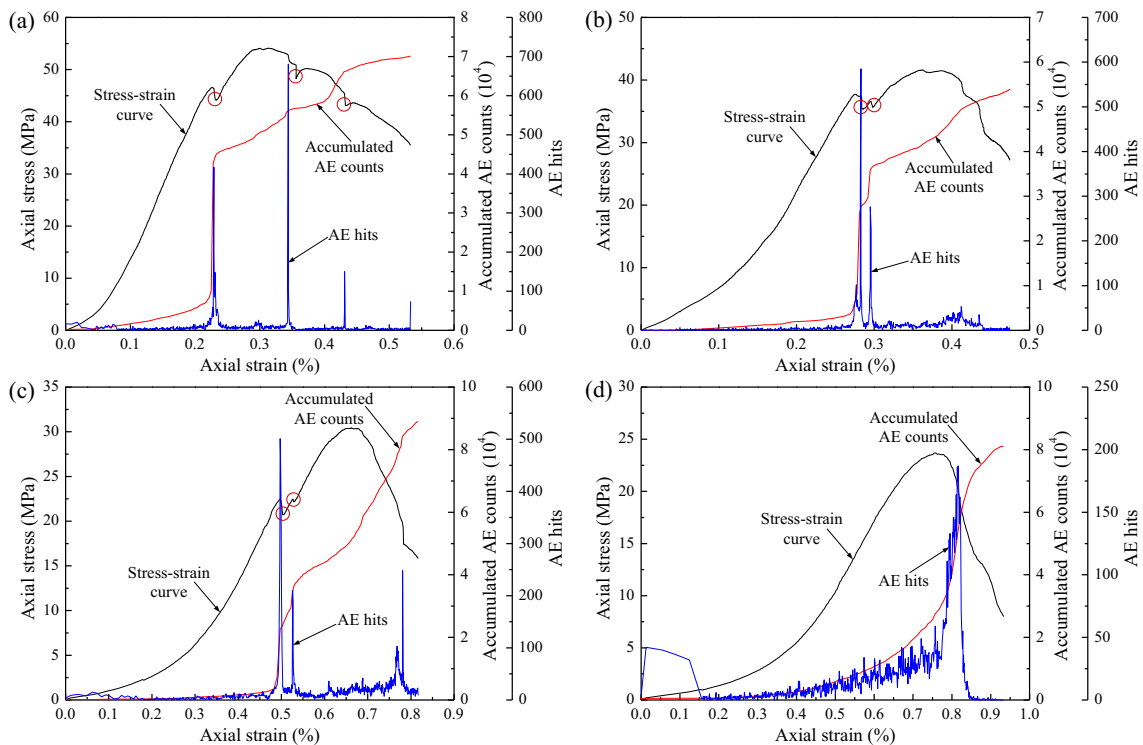


Fig. 5 Evolutions of accumulated AE counts and AE hits with axial strain for rock specimens with 75 mm diameter after thermal treatment with different temperatures. **a** Room temperature (25 °C), **b** 200 °C, **c** 400 °C, and **d** 600 °C

counts shows a slight decrease for specimens with a diameter of 75 mm, the AE hits increases two- to three-fold. It is also indicated that more AE signals will be generated in large specimens as compared with small specimens.

Specimens with a diameter of 100 mm

Figure 6 presents the stress–strain relations and the corresponding variations of accumulated AE counts and AE hits with the axial strain for specimens with a diameter of 100 mm. It is seen that the recorded AE parameters correlate well with the micro-cracking process in the rock specimen during loading. The evolution of AE parameters can divide the rock deformation into several stages, which is in good agreement with the progressive failure in the stress–strain curve. Similar to the specimens with other diameters, the AE signals in the initial deformation stage will become more prominent with the increase in the treatment temperature for specimens with a diameter of 100 mm. In addition, the “sudden stress drop” phenomenon, which denotes the dislocation or breakage of minerals or grain boundary movement in the rock specimen, can also be observed (see the red circles in Fig. 6). The numbers of accumulated AE counts and AE hits of specimens with a diameter of 100 mm show a significant increase when compared

with those of specimens with other diameters. The results reveal that more AE signals will be generated in large specimens as compared with small specimens.

Relationships between accumulated AE parameters with temperature

This section examines the variations of accumulated AE parameters, such as AE counts, AE hits, and AE energy, in response to the change of treatment temperature. To have a fair comparison of the test results, the AE parameters corresponding to the peak strength point in the stress–strain curve are examined for all the specimens.

Figure 7 presents the variations of accumulated AE counts with the treatment temperature. The details are summarized in Table 2. The results reveal that the accumulated AE counts generally decrease as the treatment temperature gradually increases. This is because more thermally induced micro-cracks will be generated inside the rock specimen with the increase in the treatment temperature. These initially generated micro-cracks will weaken the rock (i.e., lower the rock strength and Young’s modulus) (Rong et al. 2018c). Fewer AE signals (i.e., micro-cracking) will be detected upon failure of the

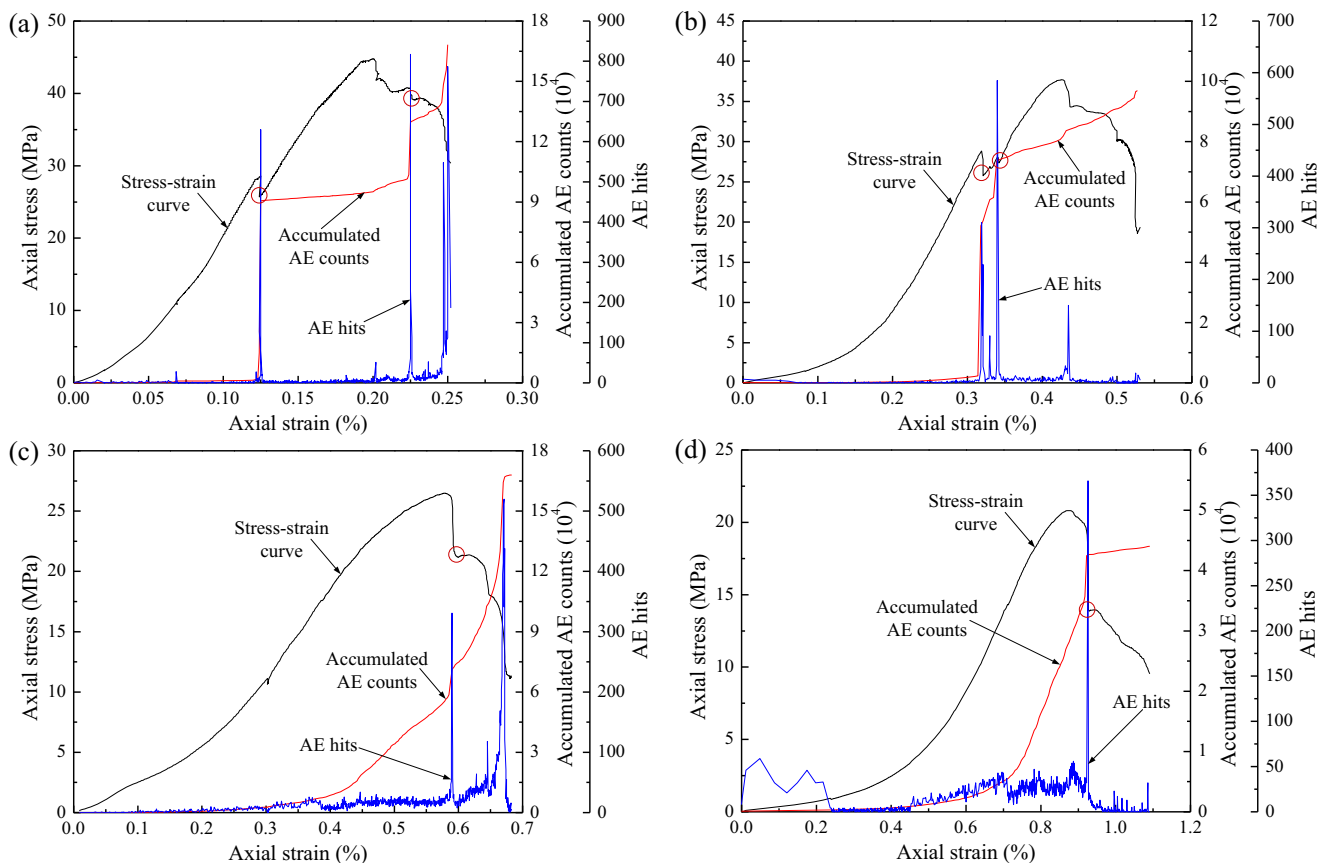


Fig. 6 Evolutions of accumulated AE counts and AE hits with axial strain for rock specimens with 100 mm diameter after thermal treatment with different temperatures. **a** Room temperature (25 °C), **b** 200 °C, **c** 400 °C, and **d** 600 °C

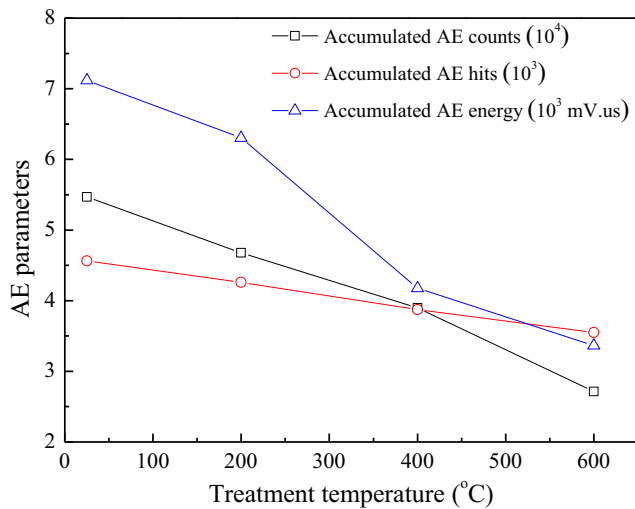


Fig. 7 Variation of different AE parameters with the treatment temperature

specimen, leading to a decrease of the number of accumulated AE counts with increasing temperature.

The variations of accumulated AE hits with the treatment temperature are also shown in Fig. 7. It is seen that, with the increase in the treatment temperature, the accumulated AE hits generally show a decreasing trend, which is mainly associated with the initial thermally induced micro-cracks inside the rock specimen.

It is generally accepted that the energy of an AE signal represents a part of the energy released in the source. The parameter is considered to be representative of the intensity of an AE event and has become widely used to study the brittle failure of rocks (Keshavarz et al. 2010; Kong et al. 2016; Zhang et al. 2015a). In this study, the accumulated AE energy corresponding to the peak stress of rock specimens is investigated. Figure 7 also presents the variations of accumulated AE energy in response to the change of treatment temperature. The results reveal that the accumulated AE energy generally shows a decreasing trend with the increase in the treatment temperature. The results of accumulated AE energy are in good agreement with those of accumulated AE counts and hits as described above.

Variation of b -value along rock deformation

The b -value of rock specimens with different diameters and different degrees of thermal damage is examined in this section. As shown in Fig. 8, the b -value generally shows a decreasing trend with the increase in the normalized axial stress. The b -value can represent the intensity of AE events in the material and a low b -value corresponds to intensive AE activities. It is indicated that the AE signals are not prominent in the initial deformation stage and gradually initiate and propagate upon approaching the peak stress.

The results shown in Fig. 8 also reveal that the b -value generally increases with the increase in the treatment temperature. The AE activities in rock specimens with lower treatment temperature are more intensive than those with higher treatment temperature. This phenomenon is mainly due to the greater number of micro-cracks residing inside the rock specimen with higher treatment temperature. These initially developed thermal micro-cracks will weaken the rock specimen and lead to a less intensive micro-cracking (i.e., AE events) when the specimen is mechanically loaded. The results are in good agreement with the observations in uniaxial compression tests (Rong et al. 2018c).

In addition, the b -value is sometimes found to drop suddenly and then recover to a higher value quickly (see the solid circles in Fig. 8), which denotes drastic AE activities at that stage. By comparing the deformation process of rock specimens (i.e., Figs. 3, 4, 5, and 6), it is seen that these events correspond well with these “sudden stress drops” in the stress–strain curve. Hence, the phenomenon is mainly attributed to the dislocation or breakage of minerals or grain boundary movement in the rock specimen.

Micro-cracking evolution

The real-time source location method can be used to determine the micro-cracking evolutions of rock specimens during loading, which provides a better visualization for interpretation of the micro-cracking process. As two examples,

Table 2 Calculated AE parameters of rock specimens with different diameters and different treatment temperatures

D (mm)	Accumulated AE energy (mV· μ s)				Accumulated AE hits				Accumulated AE counts			
	T (°C) = 25	200	400	600	25	200	400	600	25	200	400	600
25	4663	6492	3395	4377	2442	2017	2640	2189	11,325	17,234	20,420	23,589
50	5779	4633	3454	2182	7791	6270	4264	4338	60,571	46,450	29,619	30,011
75	9983	8663	3901	3998	5183	5434	4859	4324	51,784	41,705	51,045	27,419
100	8044	5432	5960	2897	2831	3321	3727	3344	95,084	81,769	54,823	27,601
Average	7117	6305	4178	3364	4562	4261	3873	3549	54,691	46,790	38,977	27,155

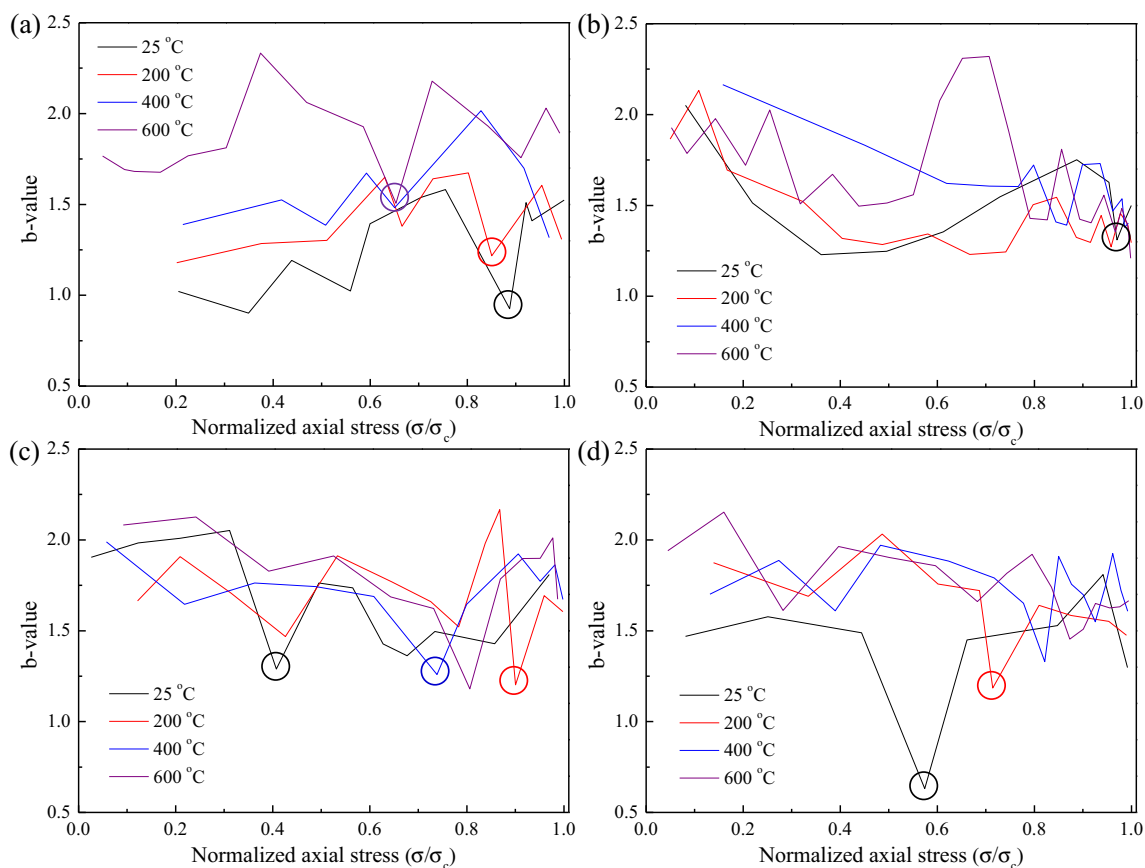


Fig. 8 Variations of the b -value of specimens possessing different degrees of thermal damages with the normalized axial stress. Specimen diameters of: **a** 25, **b** 50, **c** 75, and **d** 100 mm

Figs. 9 and 10 present the evolutions of accumulated AE events in the rock specimens at different deformation stages for a specimen with a diameter of 50 mm and no thermal damage (25 °C) and for a specimen with a diameter of 100 mm and treated under the temperature of 600 °C, respectively.

As shown in Fig. 9, the AE counts gradually initiate and multiply as the specimen is loaded to failure. The AE events cloud will finally form a general macroscopic failure plane in the specimen. For the rock specimen with a diameter of 50 mm and without thermal damage, the formed failure plane shown in the AE counts cloud is generally oriented in the axial direction, representing splitting failure (see the blue dashed line). This result is in good agreement with that observed in laboratory tests, as shown in Fig. 9c. It is indicated that the spatial distribution of AE events correlates well with the failure plane observed in uniaxial compression tests.

The results shown in Fig. 10 also reveal that the interpreted failure plane in the AE counts cloud is comparable with that observed in the uniaxial compression test. For the rock specimen with a diameter of 100 mm and treated under the temperature of 600 °C, the failure is found to be associated with a single shear

failure plane, which is different from that of the specimen with a diameter of 50 mm and without thermal damage. This observation is similar to previous laboratory test results on thermally damaged rocks (Guo et al. 2015; Kong et al. 2016).

It is also seen from Fig. 10 that the number of located AE counts for the rock specimen with a diameter of 100 mm and treated under the temperature of 600 °C is lower than that for the specimen with a diameter of 50 mm and without thermal damage. This observation is in good agreement with the results from AE parameters studies mentioned above.

It is well known that the results of AE source location is affected by many factors, such as source location algorithm, determination of arrival time, setting of wave velocity, inhomogeneity of the specimen, specimen size, actual position of the transducer, coupling agent, and ambient noise. To minimize the results error of the AE source location, special attention should be paid to the above-mentioned factors. As pointed out by Labuz et al. (1988), at least four AE transducers should be used to determine the locations of AE sources for a cylindrical specimen. When four AE transducers are used, there is no degree of freedom of the AE location system and only a unique set of solutions can be achieved. However, by comparing the located AE counts with the actual failure

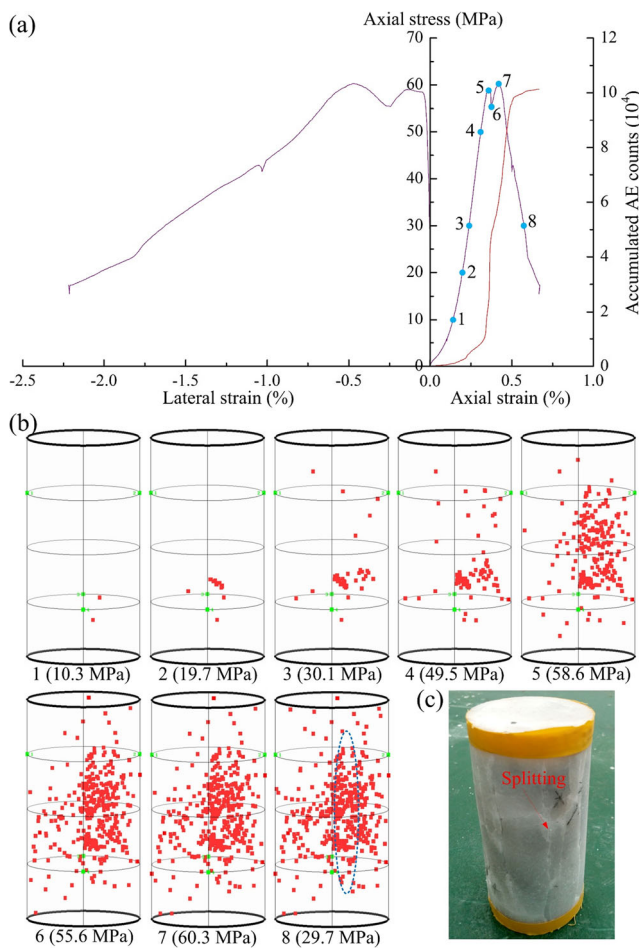


Fig. 9 Locations of accumulated AE events in a rock specimen (50 mm diameter, no thermal damage) at different deformation stages. **a** Complete stress–strain curve associated with the evolution of AE counts (the numbers on the stress–strain curve denote different stress levels); **b** spatial distribution of accumulated AE counts in the specimen (numbers 1 to 8 correspond to stresses at 10.3, 19.7, 30.1, 49.5, 58.6, 55.6, 60.3, and 29.7 MPa, respectively); **c** experimentally observed splitting fracture approximately parallel to the loading direction

pattern, a result error of 10 mm is estimated for the AE source location.

Conclusions

This paper experimentally investigates the acoustic emission (AE) characteristics of a fine-grained marble with different thermal damages and specimen sizes. The results in this study reveal that the AE technique provides useful information on the micro-cracking behavior involved in the deformation process of rocks. Based on the test results, the following conclusions can be drawn.

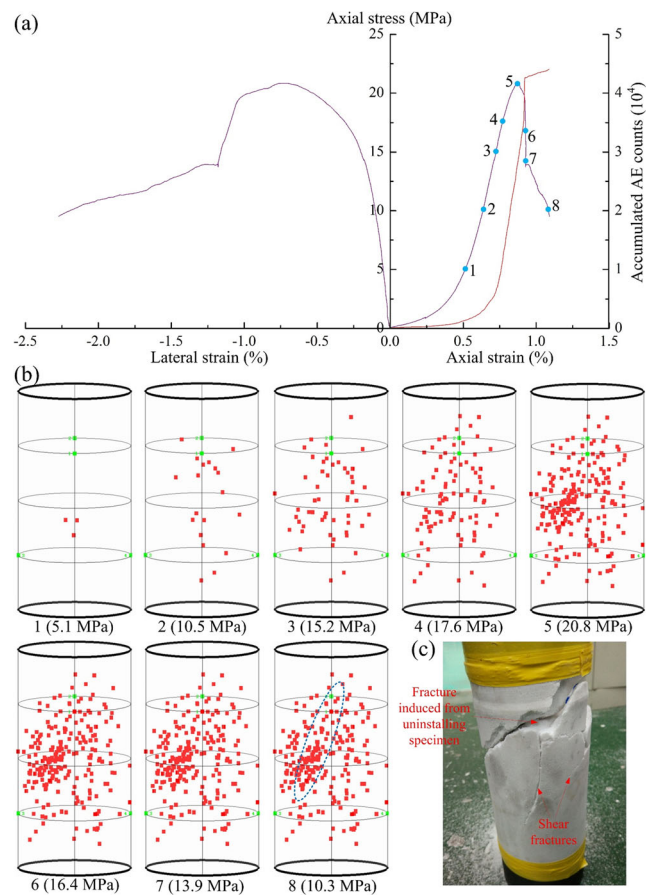


Fig. 10 Locations of accumulated AE events in a rock specimen (100 mm diameter, thermally damaged under the temperature of 600 °C) at different deformation stages. **a** Complete stress–strain curve associated with the evolution of AE counts (the numbers on the stress–strain curve denote different stress levels); **b** spatial distribution of accumulated AE counts in the specimen (numbers 1 to 8 correspond to stresses at 5.1, 10.5, 15.2, 17.6, 20.8, 16.4, 13.9, and 10.3 MPa, respectively); **c** experimentally observed shear fracture in the specimen

1. It is seen from the variation of AE counts in response to the rock deformation that the stress–strain relation can be divided into several stages. The AE activity is rare in the initial deformation stage, which then multiplies at a stress level about 0.7 to 0.8 times the peak stress. However, the AE activities in the initial deformation stage are found to be more prominent in the rock specimens which have been thermally treated.
2. The AE parameters, such as accumulated AE counts, AE hits, and AE energy, are found to generally decrease with the increase in the treatment temperature. The *b*-value generally decreases in the deformation process and correlates well with the stress–strain relation. The *b*-value is also found to generally increase with the increase in the treatment temperature, which is mainly attributed to the initially generated thermal micro-cracks in the rock specimen. The spatial distribution of AE events is in

considerable agreement with the failure plane observed in laboratory compressive tests.

Acknowledgements The research work presented in this paper is, in part, supported by the National Natural Science Foundation of China (grant nos. 51609178, 51579189, and 41772305), the Fundamental Research Funds for the Central Universities (grant nos. 2042016kf0042 and 2042016kf0171), the Natural Science Foundation of Hubei Province (grant no. 2018CFB593), the China Postdoctoral Science Foundation (grant nos. 2015M582273 and 2018T110800), and the Open-end Research Fund of the State Key Laboratory for Geomechanics and Deep Underground Engineering (grant no. SKLGDUEK1709). The fourth author also acknowledges the support of the “China University of Geosciences Scholar” Program (2017046). The authors are grateful for these financial supports.

References

- Aker E, Kühn D, Vavryčuk V, Soldal M, Oye V (2014) Experimental investigation of acoustic emissions and their moment tensors in rock during failure. *Int J Rock Mech Min Sci* 70:286–295
- Alcott JM, Kaiser PK, Simser BP (1998) Use of microseismic source parameters for rockburst hazard assessment. *Pure Appl Geophys* 153:41–65
- Bieniawski ZT (1967) Mechanism of brittle fracture of rock: part I—theory of the fracture process. *Int J Rock Mech Min Sci Geomech Abstr* 4(4):395–430
- Brace WF, Paulding BW Jr, Scholz CH (1966) Dilatancy in the fracture of crystalline rocks. *J Geophys Res* 71:3939–3953
- Butt SD, Mukherjee C, Lebas G (2000) Evaluation of acoustic attenuation as an indicator of roof stability in advancing headings. *Int J Rock Mech Min Sci* 37:1123–1131
- Cai M, Kaiser PK, Tasaka Y, Maejima T, Morioka H, Minami M (2004) Generalized crack initiation and crack damage stress thresholds of brittle rock masses near underground excavations. *Int J Rock Mech Min Sci* 41(5):833–847
- Chang SH, Lee CI (2004) Estimation of cracking and damage mechanisms in rock under triaxial compression by moment tensor analysis of acoustic emission. *Int J Rock Mech Min Sci* 41:1069–1086
- Chen L, Wang CP, Liu JF, Liu J, Wang J, Jia Y, Shao JF (2015) Damage and plastic deformation modeling of Beishan granite under compressive stress conditions. *Rock Mech Rock Eng* 48(4):1623–1633
- Chen G, Li T, Guo F, Wang Y (2017) Brittle mechanical characteristics of hard rock exposed to moisture. *Bull Eng Geol Environ* 76(1):219–230
- Dai F, Li B, Xu NW, Fan YL, Zhang CQ (2016) Deformation forecasting and stability analysis of large-scale underground powerhouse caverns from microseismic monitoring. *Int J Rock Mech Min Sci* 86:269–281
- Diederichs MS, Martin CD (2010) Measurement of spalling parameters from laboratory testing. In: *Proceedings of the ISRM International Symposium—EUROCK, Lausanne, Switzerland, June 2010*
- Diederichs MS, Kaiser PK, Eberhardt E (2004) Damage initiation and propagation in hard rock during tunnelling and the influence of near-face stress rotation. *Int J Rock Mech Min Sci* 41(5):785–812
- Eberhardt E, Stead D, Stimpson B, Read RS (1997) Changes in acoustic event properties with progressive fracture damage. *Int J Rock Mech Min Sci* 34(3–4):071B
- Eberhardt E, Stead D, Stimpson B, Read RS (1998) Identifying crack initiation and propagation thresholds in brittle rock. *Can Geotech J* 35(2):222–233
- Eberhardt E, Stimpson B, Stead D (1999) Effects of grain size on the initiation and propagation thresholds of stress-induced brittle fractures. *Rock Mech Rock Eng* 32(2):81–99
- Filimonov YL, Lavrov AV, Shafarenko YM, Shkuratnik VL (2001) Memory effects in rock salt under triaxial stress state and their use for stress measurement in a rock mass. *Rock Mech Rock Eng* 34(4):275–291
- Fu X, Xie Q, Liang L (2015) Comparison of the Kaiser effect in marble under tensile stresses between the Brazilian and bending tests. *Bull Eng Geol Environ* 74(2):535–543
- Goodfellow SD, Young RP (2014) A laboratory acoustic emission experiment under in situ conditions. *Geophys Res Lett* 41(10):3422–3430
- Guo QL, Rong G, Yao MD, Cheng L, Yang J, Peng J (2015) Experimental study on acoustic emission characteristics and mechanical behaviours of thermally damaged marble. *Chin J Rock Mech Eng* 34(12):2388–2400 (in Chinese)
- Gutenberg B, Richter CF (1942) Earthquake magnitude, intensity, energy, and acceleration. *Bull Seismol Soc Am* 32:163–191
- Hawkins AB (1998) Aspects of rock strength. *Bull Eng Geol Environ* 57:17–30
- He MC, Miao JL, Feng JL (2010) Rock burst process of limestone and its acoustic emission characteristics under true-triaxial unloading conditions. *Int J Rock Mech Min Sci* 47:286–298
- Jansen DP, Carlson SR, Young RP, Hutchins DA (1993) Ultrasonic imaging and acoustic emission monitoring of thermally induced microcracks in Lac du Bonnet granite. *J Geophys Res Solid Earth* 98(B12):22231–22243
- Keshavarz M, Pellet FL, Loret B (2010) Damage and changes in mechanical properties of a gabbro thermally loaded up to 1,000 C. *Pure Appl Geophys* 167(12):1511–1523
- Kim JS, Lee KS, Cho WJ, Choi HJ, Cho GC (2015) A comparative evaluation of stress–strain and acoustic emission methods for quantitative damage assessments of brittle rock. *Rock Mech Rock Eng* 48(2):495–508
- Koerner RM, McCabe WM, Lord AE (1981) Overview of acoustic emission monitoring of rock structures. *Rock Mech* 14:27–35
- Kong B, Wang E, Li Z, Wang X, Liu J, Li N (2016) Fracture mechanical behavior of sandstone subjected to high-temperature treatment and its acoustic emission characteristics under uniaxial compression conditions. *Rock Mech Rock Eng* 49(12):4911–4918
- Labuz JF, Chang HS, Dowding CH, Shah SP (1988) Parametric study of acoustic emission location using only four sensors. *Rock Mech Rock Eng* 21:139–148
- Lajtai EZ, Lajtai VN (1974) The evolution of brittle fracture in rocks. *J Geol Soc* 130(1):1–16
- Lei XL, Kusunose K, Nishizawa O, Cho A, Satoh T (2000) On the spatio-temporal distribution of acoustic emissions in two granitic rocks under triaxial compression: the role of pre-existing cracks. *Geophys Res Lett* 27(13):1997–2000
- Lei X, Masuda K, Nishizawa O, Jouniaux L, Liu L, Ma W, Satoh T, Kusunose K (2004) Detailed analysis of acoustic emission activity during catastrophic fracture of faults in rock. *J Struct Geol* 26:247–258
- Liu Q, Qian Z, Wu Z (2017) Micro/macro physical and mechanical variation of red sandstone subjected to cyclic heating and cooling: an experimental study. *Bull Eng Geol Environ*. <https://doi.org/10.1007/s10064-017-1196-z>
- Lockner D (1993) The role of acoustic emission in the study of rock fracture. *Int J Rock Mech Min Sci Geomech Abstr* 30:883–899
- Lockner D, Byerlee JD, Kuksenko V, Ponomarev A, Sidorin A (1991) Quasi-static fault growth and shear fracture energy in granite. *Nature* 350:39–42
- Mansurov VA (1994) Acoustic emission from failing rock behaviour. *Rock Mech Rock Eng* 27(3):173–182
- Martin CD, Chandler NA (1994) The progressive fracture of Lac du Bonnet granite. *Int J Rock Mech Min Sci Geomech Abstr* 31(6):643–659
- Meng F, Zhou H, Wang Z, Zhang L, Kong L, Li S, Zhang C, Hu S (2017) Experimental study of factors affecting fault slip rockbursts in

- deeply buried hard rock tunnels. *Bull Eng Geol Environ* 76(3): 1167–1182
- Mogi K (1962) Magnitude–frequency relation for elastic shocks accompanying fractures of various materials and some related problems in earthquakes. *Bull Earthq Res Inst Univ Tokyo* 40:831–853
- Pei JL, Liu JF, Zuo JP, Zhang R (2013) Investigation on dynamic evolution process of natural fractures based on acoustic emission position. *Chin J Rock Mech Eng* 32(4):696–704 (in Chinese)
- Peng J, Rong G, Cai M, Yao MD, Zhou CB (2016a) Physical and mechanical behaviors of a thermal-damaged coarse marble under uniaxial compression. *Eng Geol* 200:88–93
- Peng J, Rong G, Cai M, Yao MD, Zhou CB (2016b) Comparison of mechanical properties of undamaged and thermal-damaged coarse marbles under triaxial compression. *Int J Rock Mech Min Sci* 83: 135–139
- Rong G, Yao M, Peng J, Sha S, Tan J (2018a) Influence of initial thermal cracking on physical and mechanical behaviour of a coarse marble: insights from uniaxial compression tests with acoustic emission monitoring. *Geophys J Int* 214:1886–1900
- Rong G, Peng J, Cai M, Yao M, Zhou C, Sha S (2018b) Experimental investigation of thermal cycling effect on physical and mechanical properties of bedrocks in geothermal fields. *Appl Therm Eng* 141: 174–185
- Rong G, Peng J, Yao M, Jiang Q, Wong LNY (2018c) Effects of specimen size and thermal-damage on physical and mechanical behavior of a fine-grained marble. *Eng Geol* 232:46–55
- Scholz CH (1968a) Microfracturing and the inelastic deformation of rock in compression. *J Geophys Res* 73(4):1417–1432
- Scholz CH (1968b) The frequency–magnitude relation of microfracturing in rock and its relation to earthquakes. *Bull Seismol Soc Am* 58(1): 399–415
- Shao S, Ranjith PG, Wasantha PLP, Chen BK (2015) Experimental and numerical studies on the mechanical behaviour of Australian Strathbogie granite at high temperatures: an application to geothermal energy. *Geothermics* 54:96–108
- Sirdesai NN, Mahanta B, Ranjith PG, Singh TN (2017a) Effects of thermal treatment on physico-morphological properties of Indian fine-grained sandstone. *Bull Eng Geol Environ*. <https://doi.org/10.1007/s10064-017-1149-6>
- Sirdesai NN, Singh TN, Gamage RP (2017b) Thermal alterations in the poro-mechanical characteristic of an Indian sandstone—a comparative study. *Eng Geol* 226:208–220
- Sirdesai NN, Singh TN, Ranjith PG, Singh R (2017c) Effect of varied durations of thermal treatment on the tensile strength of red sandstone. *Rock Mech Rock Eng* 50(1):205–213
- Sirdesai NN, Gupta T, Singh TN, Ranjith PG (2018a) Studying the acoustic emission response of an Indian monumental sandstone under varying temperatures and strains. *Constr Build Mater* 168:346–361
- Sirdesai NN, Singh A, Sharma LK, Singh R, Singh TN (2018b) Determination of thermal damage in rock specimen using intelligent techniques. *Eng Geol* 239:179–194
- Slatalla N, Alber M, Kahraman S (2010) Analyses of acoustic emission response of a fault breccia in uniaxial deformation. *Bull Eng Geol Environ* 69(3):455–463
- Tapponnier P, Brace WF (1976) Development of stress-induced microcracks in Westerly granite. *Int J Rock Mech Min Sci Geomech Abstr* 13:103–112
- Vinegar HJ, De Waal JA, Wellington SL (1991) CT studies of brittle failure in Castlegate sandstone. *Int J Rock Mech Min Sci Geomech Abstr* 28(5):441–450
- Wong LNY, Einstein HH (2009a) Crack coalescence in molded gypsum and Carrara marble: part 1. Macroscopic observations and interpretation. *Rock Mech Rock Eng* 42(3):475–511
- Wong LNY, Einstein HH (2009b) Crack coalescence in molded gypsum and Carrara marble: part 2—microscopic observations and interpretation. *Rock Mech Rock Eng* 42(3):513–545
- Xie HP, Liu JF, Ju Y, Li J, Xie LZ (2011) Fractal property of spatial distribution of acoustic emissions during the failure process of bedded rock salt. *Int J Rock Mech Min Sci* 48:1344–1351
- Xiong Q, Wong LNY (2017) Comparison of three source types for calibrating AE sensors used in fracture coalescence tests. In: *Proceedings of the 51st US Rock Mechanics/Geomechanics Symposium (ARMA2017)*, San Francisco, California, USA, June 2017, paper no. ARMA-2017-1015
- Xu NW, Li TB, Dai F, Zhang R, Tang CA, Tang LX (2016) Microseismic monitoring of strainburst activities in deep tunnels at the Jinping II hydropower station, China. *Rock Mech Rock Eng* 49(3):981–1000
- Xu NW, Dai F, Li B, Zhu YG, Zhao T, Yang DS (2017) Comprehensive evaluation of excavation-damaged zones in the deep underground caverns of the Houziyan hydropower station, Southwest China. *Bull Eng Geol Environ* 76(1):275–293
- Yan P, Lu W, He Y, Zhou W, Chen M, Wang G (2016) Coring damage mechanism of the Yan-tang group marble: combined effect of stress redistribution and rock structure. *Bull Eng Geol Environ* 75(4): 1701–1716
- Yang SQ, Jing HW, Wang SY (2012) Experimental investigation on the strength, deformability, failure behavior and acoustic emission locations of red sandstone under triaxial compression. *Rock Mech Rock Eng* 45(4):583–606
- Zhai S, Wu G, Zhang Y, Luo C, Li Y (2013) Research on acoustic emission characteristics of granite under high temperature. *Chin J Rock Mech Eng* 32(1):126–134 (in Chinese)
- Zhang R, Dai F, Gao MZ, Xu NW, Zhang CP (2015a) Fractal analysis of acoustic emission during uniaxial and triaxial loading of rock. *Int J Rock Mech Min Sci* 79:241–249
- Zhang C, Liang W, Li Z, Xu S, Zhao Y (2015b) Observations of acoustic emission of three salt rocks under uniaxial compression. *Int J Rock Mech Min Sci* 77:19–26
- Zhao F, He MC (2017) Size effects on granite behavior under unloading rockburst test. *Bull Eng Geol Environ* 76(3):1183–1197
- Zhao XG, Cai M, Wang J, Ma LK (2013) Damage stress and acoustic emission characteristics of the Beishan granite. *Int J Rock Mech Min Sci* 64:258–269
- Zhao XG, Wang J, Cai M, Cheng C, Ma LK, Su R, Zhao F, Li DJ (2014) Influence of unloading rate on the strainburst characteristics of Beishan granite under true-triaxial unloading conditions. *Rock Mech Rock Eng* 47(2):467–483
- Zhao XG, Cai M, Wang J, Li PF (2015) Strength comparison between cylindrical and prism specimens of Beishan granite under uniaxial compression. *Int J Rock Mech Min Sci* 76:10–17